Band filling and correlation controlling electronic properties and magnetism in $K_xFe_{2-y}Se_2$: a slave boson study

2013 J. Phys.: Condens. Matter 25 125601

(http://iopscience.iop.org/0953-8984/25/12/125601)

J. Phys.: Condens. Matter **25** (2013) 125601 (11pp) doi:10.1088/0953-8984/25/12/125601

Band filling and correlation controlling electronic properties and magnetism in $K_xFe_{2-y}Se_2$: a slave boson study

Da-Yong Liu, Ya-Min Quan, Xiao-Jun Zheng, Xiang-Long Yu and Liang-Jian Zou

Key Laboratory of Materials Physics, Institute of Solid State Physics, Chinese Academy of Sciences, PO Box 1129, Hefei 230031, People's Republic of China

E-mail: zou@theory.issp.ac.cn

Received 8 November 2012, in final form 29 December 2012
Published 19 February 2013
Online at stacks.iop.org/JPhysCM/25/125601

Abstract

We investigate the electronic and magnetic properties of $K_xFe_{2-y}Se_2$ materials at different band fillings utilizing the multi-orbital Kotliar–Ruckenstein slave boson mean-field approach. We find that the ground state of KFe_2Se_2 is a paramagnetic (PM) bad metal with intermediate correlation, in contrast with the previous antiferromagnetic (AFM) results obtained by the local density approximation. Our PM metallic ground state suggests that KFe_2Se_2 is the parent phase of superconducting $K_xFe_{2-y}Se_2$, supporting a recent scanning tunneling spectroscopy experiment. For pure Fe^{2+}-based systems, the ground state is a striped AFM (SAFM) metal with a spin density wave gap partially opened near the Fermi level. In comparison, for Fe^{3+}-based compounds, besides SAFM, a Néel AFM metal without orbital ordering is observed, and an orbital selective Mott phase (OSMP) accompanied by an intermediate-spin to high-spin transition is also found, giving a possible scenario of an OSMP in $K_xFe_{2-y}Se_2$. These results demonstrate that the band filling and correlation control the Fermi surface topology, electronic state and magnetism in $K_xFe_{2-y}Se_2$.

(Some figures may appear in colour only in the online journal)

1. Introduction

Recently a new iron selenide superconductor $K_xFe_{2-y}Se_2$ with T_c above 30 K [1] has attracted considerable attention owing to its unique high Néel transition temperature and insulating properties, as well as the presence of intrinsic Fe-vacancy ordering [2–5], quite different from the other iron-based superconducting materials. These unusual properties have led to an assumption that $K_xFe_{2-y}Se_2$ may be a strongly correlated system. KFe_2Se_2 is isostructural to the 122 system, e.g. $BaFe_2As_2$, but chemically is close to FeSe. On average there are 6.5 electrons with an equal ratio of Fe^{2+} and Fe^{+} in KFe_2Se_2, rather than 6 electrons in the iron-pnictide parent compounds with solely Fe^{2+}. Therefore it can be regarded as an electron overdoped 11 system, in contrast to the underdoped KFe_2As_2, which has 5.5 electrons with an equal ratio of Fe^{2+} and Fe^{3+}, and FeAs, which has 5 electrons with Fe^{3+}. As a consequence, only the electron Fermi surface (FS) pockets exist around the M points in KFe_2Se_2, as observed in recent angle-resolved photoemission spectroscopy (ARPES) experiments [6, 7] and electronic structure calculations [8, 9]. Thus, the FS nesting between the hole pocket around the Γ point and the electron pocket around the M point, which widely exists in FeAs-based materials, is absent in the KFe_2Se_2 compound. This FS topology breaks the dominant belief that the FS nesting of the hole and electron pockets is crucial for antiferromagnetic (AFM) order and superconducting pairing.

Due to its unique electronic structure properties, the magnetic properties of $K_xFe_{2-y}Se_2$ are focused on here. Because of the difficulty of preparing single crystals of pure AFe_2Se_2 (A = K, Tl, Rb, or Cs), its magnetic properties are mainly studied theoretically, but remain a debated issue, addressed in what follows: the local density

approximation (LDA) calculations suggest that KFe_2Se_2 is a striped AFM (SAFM) order, like the 1111 and 122 phases of the FeAs-based materials [9]; others [8] consider it to be a bi-collinear AFM with $(\pi/2, \pi/2)$ wavevector, similar to FeTe [10]. However, the LDA calculations suggest that $TlFe_2Se_2$ has a checkerboard AFM (π, π) order [11], while the dynamical spin susceptibility obtained within the random phase approximation (RPA) also suggest (π, π) instability in KFe_2Se_2 [12, 13]. These discrepant results show that further investigations on the magnetism are warranted to understand the unique properties in AFe_2Se_2 (A = K, Tl, Rb, or Cs) compounds.

Many recent experiments [14–21] reported the existence of a wide chemical phase separation in $K_xFe_{2-y}Se_2$ materials. A scanning tunneling spectroscopy (STS) experiment demonstrated the phase-separated component KFe_2Se_2 is the parent phase contributing to the superconductivity, and the $K_{0.8}Fe_{1.6}Se_2$ component is an Fe-vacancy order insulator [14], implying that pure KFe_2Se_2 in the normal state is more possibly a paramagnetic (PM) phase. One may notice that the different K contents in $K_xFe_{2-y}Se_2$ lead to different band fillings of Fe 3d orbitals, and hence to quite different electronic and magnetic properties. Furthermore, Chen *et al* reported that the electronic states and magnetic phase diagrams of the $K_xFe_{2-y}Se_2$ system are closely connected with the Fe valences [15]. We also notice that various theoretical magnetic configurations obtained within the first-principles calculations for AFe_2Se_2 (A = K, Tl, Rb, or Cs) do not include the Coulomb correlation correction [8, 9, 11], which implies a weak electronic correlation in AFe_2Se_2, in contrast with the intermediate electronic correlation in the FeAs-based compounds [22]. Thus some questions urgently require answering: how strong is the electronic correlation in $K_xFe_{2-y}Se_2$? What is the realistic electron filling? Moreover, how does the band filling affect the electronic properties and magnetism in $K_xFe_{2-y}Se_2$? Considering that KFe_2Se_2 is a possible parent phase of the superconducting state, we will focus on the $K_xFe_{2-y}Se_2$ system in the absence of an ordered Fe-vacancy at various electron fillings throughout this paper.

In this paper, to explore the role of electronic correlation on the ground-state properties of AFe_2Se_2, we adopt the Kotliar–Ruckenstein slave boson (KRSB) mean-field approach [22–26] to study the magnetic and electronic properties at different band fillings in K-doped iron selenides. Based on our previous LDA calculation results [12], we first present an effective three-orbital model for KFe_2Se_2, and then determine the ground states of this model at different electron fillings. We show that the ground states of $K_xFe_{2-y}Se_2$ at fillings of three quarters, two thirds and a half are a PM metallic phase, an SAFM with orbital ordering, and a Néel AFM one without orbital ordering in the intermediate and strong correlation regimes in addition to an orbital selective Mott phase (OSMP) related with an intermediate-spin to high-spin transition, respectively, showing that the band filling controls not only the FS topology, but also the electronic structure and magnetic properties of Fe-based superconducting materials. The rest of this paper is organized as follows: a three-orbital tight-binding model and the multi-orbital slave boson mean-field approach are presented in section 2; the numerical results and discussions appear in section 3; the last section is devoted to the final remarks and a summary.

2. Three-orbital tight-binding model and slave boson approach

Based on our previous electronic structure calculations [12], we find that the FS is mainly contributed by three t_{2g} orbitals, thus the system can be described by a three-orbital model [27], similar to iron pnictides [28–31]. We extract an effective three-orbital tight-binding model from our LDA band structures. The tight-binding model Hamiltonian for the three-orbital model in the momentum space is described as

$$H_0 = \sum_{k,\alpha,\beta,\sigma} (\epsilon_\alpha \delta_{\alpha\beta} + T^{\alpha\beta}(\mathbf{k})) C^\dagger_{k\alpha\sigma} C_{k\beta\sigma} - \mu \sum_{k\alpha\sigma} n_{k\alpha\sigma}, \quad (1)$$

where $T^{\alpha\beta}(\mathbf{k})$ is the kinetic energy term, ϵ_α denotes the on-site energy of the α orbital, and μ is the chemical potential determined by the electron filling. The three-orbital tight-binding fitting of the Fe 3d bands is displayed in the solid lines, in comparison with the original five bands [12] in the dotted lines, as shown in figure 1. The distance between the top of the hole-like band at the Γ point and the Fermi energy E_F is about 0.1 eV. It is clear that the band structures in KFe_2Se_2 are similar to those of LaFeAsO [32], only the position of Fermi energy E_F is shifted. Therefore this model can describe both the FeSe-based and FeAs-based systems by changing the chemical potential.

The tight-binding parameters of the three-orbital model for KFe_2Se_2 are listed in the following. The on-site energies measured from the Fermi energy for the three orbitals are $(\epsilon_1, \epsilon_2, \epsilon_3) = (-511.92, -511.92, -341.63)$, respectively, in units of meV. Here, the orbital indices (1, 2, 3) indicate the d_{xz}, d_{yz}, and d_{xy} components, respectively. Similar to $BaFe_2As_2$ [33], the orbital-dependent kinetic energy matrix elements are expressed in terms of the inter-orbital and intra-orbital hopping integrals as follows,

$$\begin{aligned}
T^{11/22} &= 2t^{11}_{x/y}\cos k_x + 2t^{11}_{y/x}\cos k_y + 4t^{11}_{xy}\cos k_x \cos k_y \\
&\pm 2t^{11}_{xx}(\cos 2k_x - \cos 2k_y) + 4t^{11}_{xxy/xyy}\cos 2k_x \cos k_y \\
&+ 4t^{11}_{xyy/xxy}\cos 2k_y \cos k_x + 4t^{11}_{xxyy}\cos 2k_x \cos 2k_y, \\
T^{33} &= 2t^{33}_{x}(\cos k_x + \cos k_y) + 4t^{33}_{xy}\cos k_x \cos k_y \\
&+ 2t^{33}_{xx}(\cos 2k_x + \cos 2k_y) \\
&+ 4t^{33}_{xxy}(\cos 2k_x \cos k_y + \cos 2k_y \cos k_x) \\
&+ 4t^{33}_{xxyy}\cos 2k_x \cos 2k_y, \\
T^{12} &= 4t^{12}_{xy}\sin k_x \sin k_y + 4t^{12}_{xxy}(\sin 2k_x \sin k_y + \sin 2k_y \sin k_x) \\
&+ 4t^{12}_{xxyy}\sin 2k_x \sin 2k_y, \\
T^{13/23} &= \pm 2it^{13}_{x}\sin k_{x/y} \pm 4it^{13}_{xy}\cos k_{y/x}\sin k_{x/y} \\
&\pm 4it^{13}_{xxy}\cos k_{y/x}\sin 2k_{x/y}.
\end{aligned}$$

The intra-orbital and inter-orbital hopping parameters up to the fifth nearest-neighbor for the fitting of the three-band structure in figure 1 are shown in table 1.

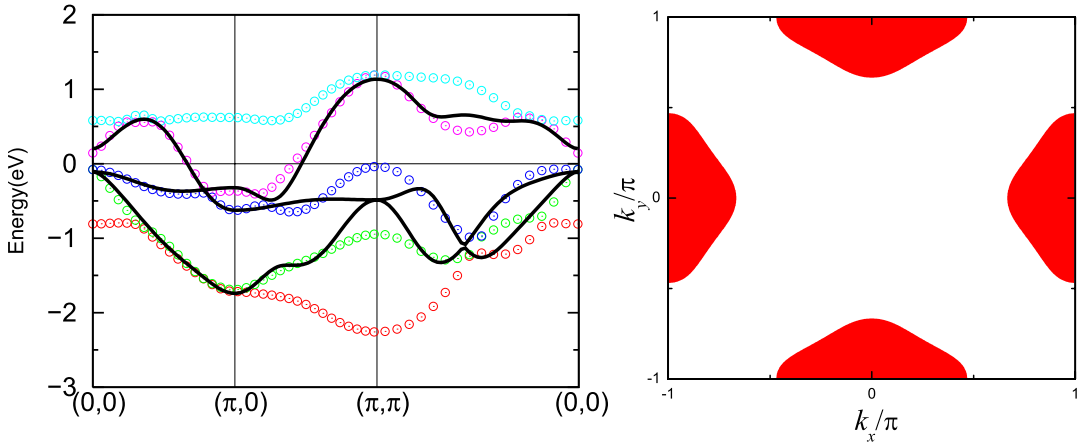

Figure 1. Left panel: the band structures of the Fe 3d orbitals obtained by the LDA and its three-orbital tight-binding fitting. Circles denote the five LDA bands [12] and solid lines the three fitted effective bands. Right panel: the corresponding Fermi surface for the parent material KFe_2Se_2 at the first Brillouin zone obtained by the three-orbital tight-binding model.

Table 1. The nonzero matrix elements of intra-orbital $t_i^{\alpha\alpha}$ and inter-orbital $t_i^{\alpha\beta}$ hopping parameters up to fifth neighbors of the three-orbital tight-binding model through fitting the band structures. All the parameters are in units of millielectronvolts.

$t_i^{\alpha\alpha}$	$i=x$	$i=y$	$i=xy$	$i=xx$	$i=xxy$	$i=xyy$	$i=xxyy$
$\alpha=1/2$	60.87	77.65	21.83	54.35	−34.35	11.97	31.67
$\alpha=3$	−53.39		301.2	21.61	−31.6		−70.04
$t_i^{\alpha\beta}$	$i=x$		$i=xy$	$i=xxy$	$i=xxyy$		
$\alpha\beta=12$			−119.57	50.99	−12.55		
$\alpha\beta=13/23$	302.39		122.5	−14.64			

Considering the Coulomb interaction, in addition to the kinetic term in equation (1), we describe the electronic interaction part of the multi-orbital Hamiltonian as follows,

$$\begin{aligned} H_I = {} & U\sum_{i,\alpha} n_{i\alpha\uparrow}n_{i\alpha\downarrow} + U'\sum_{\substack{i\\ \alpha\neq\beta}} n_{i\alpha\uparrow}n_{i\beta\downarrow} \\ & + (U'-J_{\mathrm{H}})\sum_{\substack{i,\sigma\\ \alpha<\beta}} n_{i\alpha\sigma}n_{i\beta\sigma} \\ & - J_{\mathrm{H}}\sum_{\substack{i\\ \alpha\neq\beta}} C^{\dagger}_{i\alpha\uparrow}C_{i\alpha\downarrow}C^{\dagger}_{i\beta\downarrow}C_{i\beta\uparrow} \\ & + J_{\mathrm{H}}\sum_{\substack{i\\ \alpha\neq\beta}} C^{\dagger}_{i\alpha\uparrow}C^{\dagger}_{i\alpha\downarrow}C_{i\beta\downarrow}C_{i\beta\uparrow} \end{aligned} \tag{2}$$

where $U(U')$ denotes the intra-(inter-)orbital Coulomb repulsion interaction and J_{H} the Hund's rule coupling. Considering the rotation symmetry of the system, we adopt $U' = U - 2J_{\mathrm{H}}$.

We notice that in FeAs-based materials, the electronic filling for the present three-orbital model is only at two thirds filling, i.e., for $n = 4$, the correct FS can be reproduced [30–32]. In the KFe_2Se_2 compound, the Fe ions have two kinds of valence, Fe^{2+} and Fe^{+} with equal ratio, and the average electron number is 6.5 per site, different from Fe^{2+} with 6 electrons in the FeAs-based parent materials. Consequently, pure KFe_2Se_2 should be at a filling of three quarters (i.e. $n = 4.5$), at which the FS can be reproduced correctly in the present three-orbital model. The obtained FS of KFe_2Se_2 is plotted at $k_z = 0$ in figure 1, with four electron-like FS pockets. The hole-like FS pockets at Γ are absent. Such a FS topology is in agreement with the recent ARPES experiments [6, 7] and the band structure calculations [8, 9]. To explore the band filling dependence of the electronic state, we also extend the band filling to 2/3 and 1/2, which correspond to the Fe^{2+} and Fe^{3+} systems, respectively.

The KRSB mean-field approach is known to be one of the effective methods to treat the wide electronic correlation in the many-body systems. Here, we extend the single-orbital KRSB mean-field method to the multi-orbital situation [22, 26] and apply it to $K_xFe_{2-y}Se_2$. We introduce new fermion operators $f_{i\alpha\sigma}$ slaved by boson operators $e_i, p_{i\alpha\sigma}, d_{i\alpha\sigma_\beta\sigma_\gamma}, b_{i\alpha}, t_{i\alpha\beta\sigma}, r_{i\sigma_\alpha\sigma_\beta\sigma_\gamma}, q_{i\alpha}, u_{i\alpha\sigma_\beta\sigma_\gamma}, v_{i\alpha\sigma}$ and s, which represent the empty; single occupation with α orbital and σ spin; double occupation with β orbital spin σ_β and γ orbital spin σ_γ; double occupation with two electrons in orbital α; triple occupation with two electrons in orbital α and one electron in orbital β with spin σ; triple occupation with each electron in orbital α, β and γ with spin $\sigma_\alpha, \sigma_\beta$, and σ_γ; quadruple occupation with two electrons in orbital β and γ; quadruple occupation with two electrons in orbital α, one electron in orbital β with spin σ_β and one electron in orbital γ with spin σ_γ; fivefold occupation with four electrons in orbitals β and γ, and one electron in orbital α with spin σ; and sixfold occupation, respectively.

The completeness of these boson fields gives rise to the normalization condition as follows:

$$e_i^\dagger e_i + \sum_{\alpha,\sigma} p_{i\alpha\sigma}^\dagger p_{i\alpha\sigma} + \sum_{\alpha} b_{i\alpha}^\dagger b_{i\alpha} + \sum_{\alpha,\sigma_\beta,\sigma_\gamma} d_{i\alpha\sigma_\beta\sigma_\gamma}^\dagger d_{i\alpha\sigma_\beta\sigma_\gamma} + \sum_{\sigma_\alpha,\sigma_\beta,\sigma_\gamma} r_{i\sigma_\alpha\sigma_\beta\sigma_\gamma}^\dagger r_{i\sigma_\alpha\sigma_\beta\sigma_\gamma} + \sum_{\alpha,\beta,\sigma} t_{i\alpha\beta\sigma}^\dagger t_{i\alpha\beta\sigma} + \sum_{\alpha} q_{i\alpha}^\dagger q_{i\alpha} + \sum_{\alpha,\sigma_\beta,\sigma_\gamma} u_{i\alpha\sigma_\beta\sigma_\gamma}^\dagger u_{i\alpha\sigma_\beta\sigma_\gamma} + \sum_{\alpha,\sigma} v_{i\alpha\sigma}^\dagger v_{i\alpha\sigma} + s_i^\dagger s_i = 1. \quad (3)$$

Projecting the original Hamiltonian equations (1) and (2) into the new slave boson representation, the multi-orbital Hubbard model Hamiltonian is described as:

$$\begin{aligned} H = & \sum_{i,j,\alpha,\beta,\sigma} t_{\alpha\beta}^{ij} Z_{i\alpha\sigma}^\dagger Z_{j\beta\sigma} f_{i\alpha\sigma}^\dagger f_{j\beta\sigma} + \sum_{i\alpha\sigma} (\epsilon_\alpha - \mu) f_{i\alpha\sigma}^\dagger f_{i\alpha\sigma} \\ & + U \sum_{i,\alpha} b_{i\alpha}^\dagger b_{i\alpha} + J_{\mathrm{H}} \sum_{i,\alpha}^{\alpha,\beta,\gamma} (b_{i\beta}^\dagger b_{i\gamma} + b_{i\gamma}^\dagger b_{i\beta}) \\ & + (U' - J_{\mathrm{H}}) \sum_{i,\alpha,\sigma} d_{i\alpha\sigma\bar{\sigma}}^\dagger d_{i\alpha\sigma\bar{\sigma}} + U' \sum_{i,\alpha,\sigma} d_{i\alpha\sigma\bar{\sigma}}^\dagger d_{i\alpha\sigma\bar{\sigma}} \\ & + (U + 2U' - J_{\mathrm{H}}) \sum_{i,\alpha,\sigma}^{\alpha,\beta,\gamma} (t_{i\beta\gamma\sigma}^\dagger t_{i\beta\gamma\sigma} + t_{i\gamma\beta\sigma}^\dagger t_{i\gamma\beta\sigma}) \\ & + J_{\mathrm{H}} \sum_{i,\alpha,\sigma}^{\alpha,\beta,\gamma} (t_{i\beta\alpha\sigma}^\dagger t_{i\gamma\alpha\sigma} + t_{i\beta\alpha\sigma} t_{i\gamma\alpha\sigma}^\dagger) \\ & + 3(U' - J_{\mathrm{H}}) \sum_{i,\sigma} r_{i\sigma_\alpha\sigma_\beta\sigma_\gamma}^\dagger r_{i\sigma_\alpha\sigma_\beta\sigma_\gamma} \\ & + (3U' - J_{\mathrm{H}}) \sum_{i,\alpha,\sigma}^{\alpha,\beta,\gamma} r_{a\sigma_\alpha\sigma_\beta\bar{\sigma_\gamma}}^\dagger r_{a\sigma_\alpha\sigma_\beta\bar{\sigma_\gamma}} \\ & + 2(U + 2U' - J_{\mathrm{H}}) \sum_{i,\alpha} q_{i\alpha}^\dagger q_{i\alpha} \\ & + J_{\mathrm{H}} \sum_{i,\alpha}^{\alpha,\beta,\gamma} (q_{i\beta}^\dagger q_{i\gamma} + q_{i\beta} q_{i\gamma}^\dagger) \\ & + (U + 5U' - 3J_{\mathrm{H}}) \sum_{i,\alpha,\sigma}^{\alpha,\beta,\gamma} u_{i\alpha\sigma_\beta\sigma_\gamma}^\dagger u_{i\alpha\sigma_\beta\sigma_\gamma} \\ & + (U + 5U' - 2J_{\mathrm{H}}) \sum_{i,\alpha,\sigma}^{\alpha,\beta,\gamma} u_{i\alpha\sigma_\beta\bar{\sigma_\gamma}}^\dagger u_{i\alpha\sigma_\beta\bar{\sigma_\gamma}} \\ & + (2U + 8U' - 4J_{\mathrm{H}}) \sum_{i,\alpha,\sigma} v_{i\alpha\sigma}^\dagger v_{i\alpha\sigma} \\ & + (3U + 12U' - 6J_{\mathrm{H}}) \sum_{i} s_i^\dagger s_i \end{aligned} \quad (4)$$

where the renormalization factor

$$Z_{i\alpha\sigma} = (1 - \tilde{Q}_{i\alpha\sigma})^{-\frac{1}{2}} \tilde{Z}_{i\alpha\sigma} \tilde{Q}_{i\alpha\sigma}^{-\frac{1}{2}} \quad (5)$$

$$\begin{aligned} \tilde{Z}_{i\alpha\sigma} = & e_i^\dagger p_{i\alpha\sigma} + p_{i\alpha\bar{\sigma}}^\dagger b_{i\alpha} + \sum_{\sigma'}^{\alpha,\beta,\gamma} p_{i\beta\sigma'}^\dagger d_{i\gamma\sigma\sigma'} \\ & + \sum_{\sigma'}^{\alpha,\beta,\gamma} p_{i\gamma\sigma'}^\dagger d_{i\beta\sigma'\sigma} + \sum_{\beta}^{\beta\neq\alpha} b_{i\beta}^\dagger t_{i\beta\alpha\sigma} \\ & + \sum_{\sigma',\sigma''}^{\alpha,\beta,\gamma} d_{i\alpha\sigma_\beta\sigma_\gamma}^\dagger r_{i\sigma_\alpha\sigma_\beta\sigma_\gamma} + \sum_{\sigma'}^{\alpha,\beta,\gamma} d_{i\gamma\bar{\sigma}\sigma'}^\dagger t_{i\alpha\beta\sigma'} \\ & + \sum_{\sigma\prime}^{\alpha,\beta,\gamma} d_{i\beta\sigma'\bar{\sigma}}^\dagger t_{i\alpha\gamma\sigma'} + \sum_{\sigma',\sigma''} r_{i\bar{\sigma}_\alpha\sigma_\beta\sigma_\gamma}^\dagger u_{i\alpha\sigma_\beta\sigma_\gamma} \\ & + t_{i\gamma\alpha\bar{\sigma}}^\dagger q_{i\beta} + t_{i\beta\alpha\bar{\sigma}}^\dagger q_{i\gamma} + \sum_{\sigma'} t_{i\gamma\beta\sigma'}^\dagger u_{i\gamma\sigma_\alpha\sigma_\beta} \\ & + \sum_{\sigma'} t_{i\beta\gamma\sigma'}^\dagger u_{i\beta\sigma_\gamma\sigma_\alpha} + q_{i\alpha}^\dagger v_{i\alpha\sigma} \\ & + \sum_{\sigma'} u_{i\gamma\bar{\sigma}_\alpha\bar{\sigma}_\beta}^\dagger v_{i\beta\bar{\sigma}'} + \sum_{\sigma'} u_{i\beta\sigma_\gamma\bar{\sigma}_\alpha}^\dagger v_{i\gamma\sigma'} + v_{i\alpha\bar{\sigma}}^\dagger s_i. \end{aligned} \quad (6)$$

Note that in the PM case, $Z_{i\alpha\uparrow} = Z_{i\alpha\downarrow} = Z_\alpha$; in the AFM case with A and B sublattices, $Z_{\mathrm{A}\alpha\sigma} = Z_{\mathrm{B}\alpha\bar{\sigma}} = Z_{\alpha\sigma}$. The product form $Z_{i\alpha\sigma}^\dagger Z_{j\beta\sigma'}$ represents the band narrowing factor. The corresponding fermion number constraint for the α orbital with spin σ reads:

$$\tilde{Q}_{i\alpha\sigma} = f_{i\alpha\sigma}^\dagger f_{i\alpha\sigma} \quad (7)$$

where

$$\begin{aligned} \tilde{Q}_{i\alpha\sigma} = & p_{i\alpha\sigma}^\dagger p_{i\alpha\sigma} + b_{i\alpha}^\dagger b_{i\alpha} + \sum_{\sigma'} d_{i\beta\sigma_\gamma\sigma_\alpha}^\dagger d_{i\beta\sigma_\gamma\sigma_\alpha} \\ & + \sum_{\sigma'} d_{i\gamma\sigma_\alpha\sigma_\beta}^\dagger d_{i\gamma\sigma_\alpha\sigma_\beta} + \sum_{\sigma',\sigma''} r_{i\sigma_\alpha\sigma_\beta\sigma_\gamma}^\dagger r_{i\sigma_\alpha\sigma_\beta\sigma_\gamma} \\ & + \sum_{\beta,\sigma} t_{i\alpha\beta\sigma}^\dagger t_{i\alpha\beta\sigma} + \sum_{\beta} t_{i\beta\alpha\sigma}^\dagger t_{i\beta\alpha\sigma} + \sum_{\beta}^{\beta\neq\alpha} q_{i\beta}^\dagger q_{i\beta} \\ & + \sum_{\sigma'} u_{i\gamma\sigma_\alpha\sigma_\beta}^\dagger u_{i\gamma\sigma_\alpha\sigma_\beta} + \sum_{\sigma'} u_{i\beta\sigma_\gamma\sigma_\alpha}^\dagger u_{i\beta\sigma_\gamma\sigma_\alpha} \\ & + \sum_{\sigma',\sigma''} u_{i\alpha\sigma_\beta\sigma_\gamma}^\dagger u_{i\alpha\sigma_\beta\sigma_\gamma}^\dagger \\ & + \sum_{\beta\sigma}^{\beta\neq\alpha} v_{i\beta\sigma}^\dagger v_{i\beta\sigma} + v_{i\alpha\sigma}^\dagger v_{i\alpha\sigma} + s_i^\dagger s_i. \end{aligned} \quad (8)$$

Averaging the boson operators in equations (4)–(8), we can obtain an effective mean field Hamiltonian, and hence the total ground-state energy. The original fermions are guaranteed by the constraint equation (7), which is implemented by means of the corresponding generalized Lagrange multiplier method. In order to determine the stable magnetic ground state, we minimize the total energies for different magnetic configurations based on the pattern search method. To simplify the calculations, various symmetries should be utilized. For instance, in the AFM situation with two sublattices, the single occupation probabilities $p_{\alpha\uparrow}^{\mathrm{B}}$ in sublattice B are identical to $p_{\alpha\downarrow}^{\mathrm{A}}$ in sublattice A, double occupation probabilities $d_{\alpha\downarrow\downarrow}^{\mathrm{B}} = d_{\alpha\uparrow\uparrow}^{\mathrm{A}}$, etc.

3. Results and discussions

In this section, we present the main numerical results on the electronic and magnetic properties within the three-orbital model for the iron selenide systems. Fillings of three quarters and two thirds, as well as half-filling, are all considered for comparison.

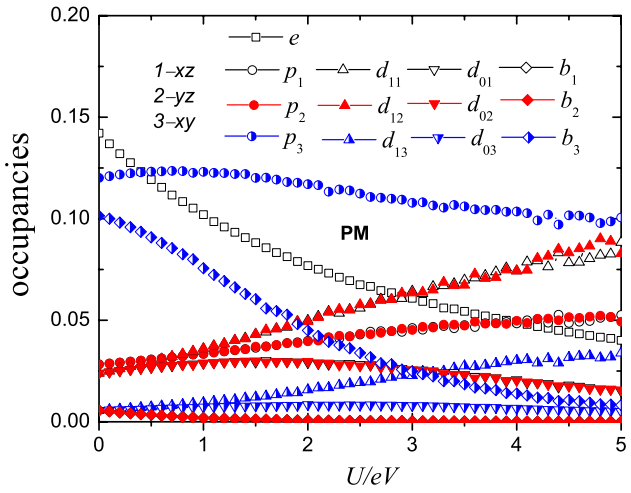

Figure 2. Dependence of boson occupancies on Coulomb interaction U at an electron filling of $n = 4.5$, and $J_H = 0.25U$. The ground state is always a PM state. Note that in the PM case, $d_{0\alpha} = d_{\alpha\uparrow\downarrow} = d_{\alpha\downarrow\uparrow}$, $d_{1\alpha} = d_{\alpha\uparrow\uparrow} = d_{\alpha\downarrow\downarrow}$.

3.1. Three quarter filling case

We firstly consider the electron filling $n = 4.5$ case, corresponding to pure KFe_2Se_2 compounds. Note that we adopt the hole representation for convenience within the KRSB mean-field approach throughout this paper. Thus the particle number in the three quarter filling case is 1.5 within the three-orbital model. Taking into account several types of magnetic configuration with high symmetry, the PM, ferromagnetic (FM), Néel AFM and SAFM cases, we find that only the PM phase is the most stable at a filling of three quarters when U increases from 0 up to 5 eV. Because of the mixing valence of Fe^{2+} and Fe^{+} in KFe_2Se_2, the system is not a magnetic ordered and insulating state in the homogeneous phase. Since the electron fillings of both Fe^{2+} and Fe^{+} are away from half-filling, unlike mixing valent $Na_{0.5}CoO_2$ [34], KFe_2Se_2 does not form charge ordering. Previous work on charge susceptibility shows that the Coulomb interaction suppresses the charge instability [12, 35], thus it is hard to form charge ordering in KFe_2Se_2.

Within the present KRSB framework, the dependence of various boson occupancies on the Coulomb interaction U at $J_H = 0.25U$ is plotted in figure 2. It is clearly found that the empty occupation e, single occupation p_3 and double occupation b_3 with orbital xy are dominant for small U. With the increase of the Coulomb interaction, the empty occupation e and triple occupation b_3 decrease sharply, while d_{11}, d_{12} and d_{13} ($d_{1\alpha} = d_{\alpha\uparrow\uparrow} = d_{\alpha\downarrow\downarrow}$) increase due to the increase of the Hund's rule coupling and the Coulomb interaction. This shows that the system is a PM, with the magnetic moment of each Fe spin increasing with a rise in U and J_H, rather than a nonmagnetic one.

The orbital occupations as a function of the Coulomb interaction are given in the left panel of figure 3. It is clearly found that the electrons occupy the lower energy xz- and yz-orbitals. Also there is no orbital polarization between the xz- and yz-orbitals. With the increase of Coulomb interaction, a fraction of electrons in the xz- and yz-orbitals transfer to the higher energy xy-orbital since the larger J_H enhances the effect of Hund's rule. Thus the high energy xy orbital is occupied by more electrons as J_H increases. The renormalization factors of each orbital as a function of the Coulomb interaction U are shown in the right panel of figure 3. With increasing Coulomb interaction, the bandwidths of the three orbitals become narrower and narrower, and the renormalization factors become small. We notice that in the PM phase the degeneracy of orbital xz and yz is not removed, and the renormalization factors of bandwidths in different orbitals are nearly the same. When U is 3, 4 and 5 eV, the renormalization factor Z is about 0.85, 0.8 and 0.76, respectively, giving rise to the band mass of original fermions $m_b/m = 1/Z^2 \sim$ 1.38, 1.56 and 1.73, respectively, and yielding a mass renormalization factor of about 2 at $U = 5$ eV. We expect that the disorder effect and the spin fluctuations beyond the KRSB mean-field approximation will further narrow the bandwidths and enhance the effective mass. This band narrowing factor is comparable with the experimental ones from ARPES [36] and de Haas–Van Alphen [37] studies, indicating that KFe_2Se_2 lies in the intermediate correlation region, similar to the FeAs-based systems. While in the presence of the Fe-vacancy, the measured renormalization factor is about 6.1 in $(Tl, Rb)_xFe_{2-y}Se_2$, very much larger than 2. This shows that most probably the insulating properties in $K_xFe_{2-y}Se_2$ systems are induced by ordering of the Fe vacancies, rather than by the strong electronic correlation.

The projected densities of states (PDOS) of KFe_2Se_2 for the Coulomb interaction $U = 0$, 1, 3 and 5 eV are shown in figure 4. It is seen in figure 4 that the DOS at the Fermi level is small but finite, while on the two sides of E_F it shows two side peaks. Such a dip structure implies that the DOS near the Fermi level exhibits a pseudo-gap-like feature. In the FeAs-based compounds, two sharp van Hove singularity peaks in the DOS are attributed to FS nesting with a wavevector $\mathbf{Q} = (\pi, 0)$ [38]. In comparison, the relatively broaden van Hove singularity peaks in the DOS of KFe_2Se_2 may be the consequence of the breakdown of the FS nesting, which arises from the fact that there are no hole pockets around Γ point. With the increase of the Coulomb interaction from 0 to 5 eV, the bandwidth becomes narrow, $W \sim 2.5$ eV at $U = 3$ eV, smaller than 3.2 eV at $U = 0$, showing that the system is a correlated bad metal and is in the intermediate correlation region with $W \sim U$.

Through the analysis above, we find that at 3/4 filling, the $K_xFe_{2-y}Se_2$ system, corresponding to KFe_2Se_2, is a PM phase. We also clarify that KFe_2Se_2 lies in an intermediate correlation region, similar to the FeAs-based compounds.

3.2. Two thirds filling case

On the other hand, the electron filling at $n = 4$ corresponds to Fe^{2+}-based compounds, such as FeSe and LaFeAsO, etc. The dependence of boson occupancy probabilities on the Coulomb interaction is also shown in figure 5. Comparing with the $n = 4.5$ case, we find that with the increase of U, the system transits from a PM metallic phase to an SAFM

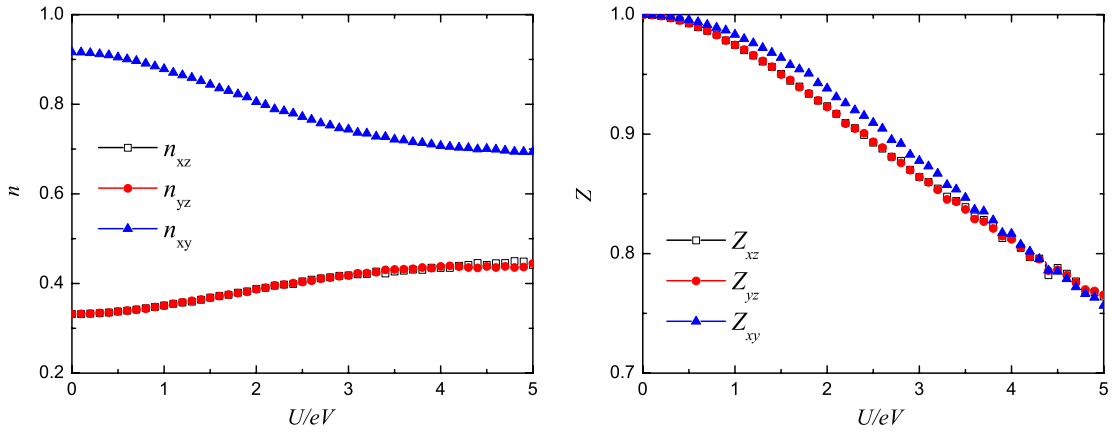

Figure 3. Orbital occupations (left panel), and renormalization factor (right panel) as a function of the Coulomb interaction U at $n = 4.5$, and $J_H = 0.25U$.

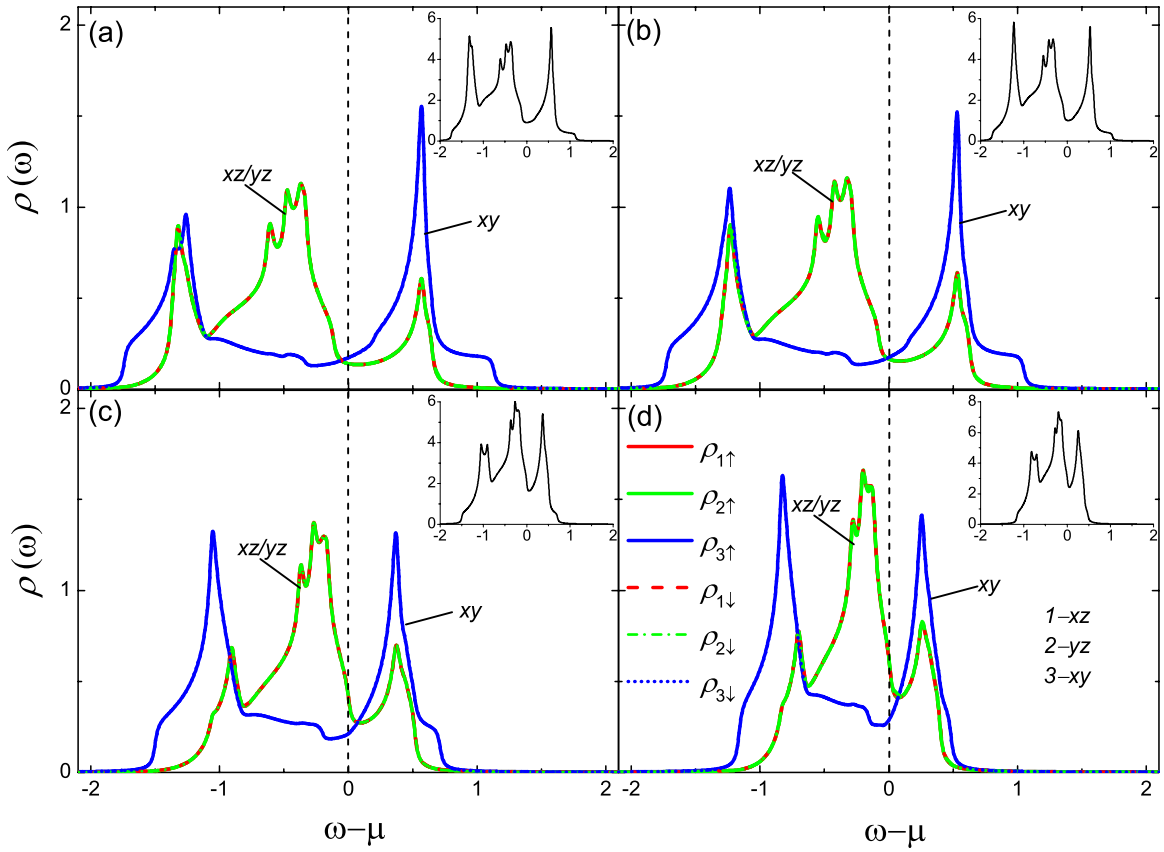

Figure 4. Projected densities of states are plotted for $U = 0$ (a), 1.0 eV (b), 3.0 eV (c), and 5.0 eV (d) at $n = 4.5$, respectively, with $J_H = 0.25U$. Inset: total densities of states.

metallic phase at a critical point $U_c \approx 1.2$ eV. In the PM phase, the single occupations in the xy-orbital p_3 and empty occupancy e are dominant. Other multiple occupation states also contribute small but finite weights. In the SAFM phase, the single, double and triple occupations with the same spin alignment, p, d and r, are dominant. The spin singlet and small spin states contribute very little. With increasing Hund's rule coupling, the empty and single occupations continuously decrease, while the double and triple occupations increase considerably. This behavior arises from the fact that the increased Coulomb interaction favors the formation of the SAFM phase, and the large Hund's rule coupling favors a large spin state.

The gap opening behavior of the SDW states in the multi-orbital FeAs-based system is an interesting but unsolved topic. In order to resolve the behavior of the SDW gap opening in $K_xFe_{2-y}Se_2$, we present the band dispersions of the PM and SDW states in figure 6. We find that in the SDW states only partial SDW gaps open near E_F in comparison with PM states, which is the consequence of the band narrowing and

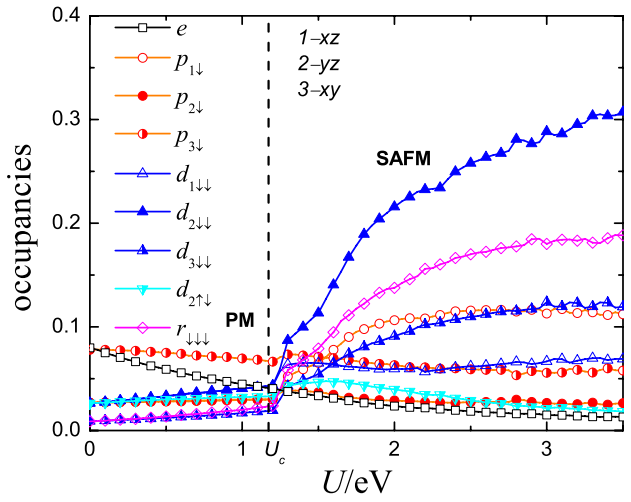

Figure 5. Dependence of various boson occupancies on the Coulomb interaction U at $n = 4$, and $J_H = 0.25U$.

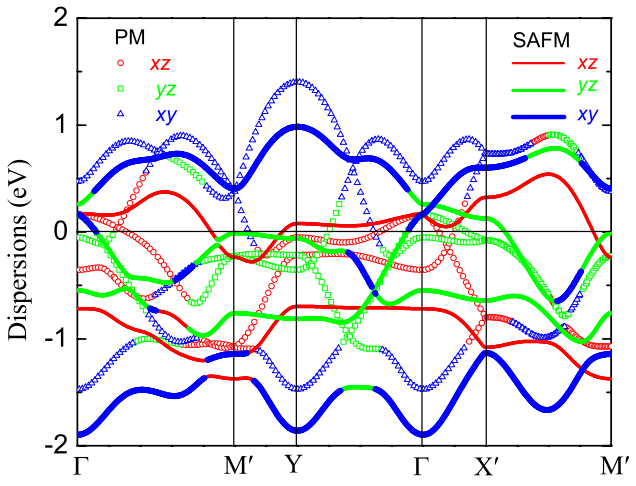

Figure 6. Band dispersions of the PM and SDW states along the high-symmetry points, $\Gamma(0, 0)$, $Y(0, \pi)$, $M'(\pi/2, \pi)$, $X'(\pi/2, 0)$, in the folded BZ with $U = 0$ and 2 eV, and $J_H = 0.25U$ at $n = 4$.

spin splitting, similar to FeAs-based compounds. The partial opening of the SDW gap indicates the system is a bad metal in the SAFM phase (SDW state).

The dependence of the orbital occupations and magnetic moment of each orbital on the Coulomb interaction U is also shown in figure 7. With an increase of U, once the system enters the SAFM phase, there is obvious orbital polarization between xz and yz orbitals together with $n_{xz} < n_{yz}$ in the electronic representation. Also the magnetic moments on the xz and yz orbitals are different, with $m_{xz} > m_{yz}$. These are consistent with the previous LaFeAsO results [22, 39]. The renormalization factors Z displayed in the right panel of figure 7 show that the $Z_{xz\uparrow}$, $Z_{yz\uparrow}$ and $Z_{xy\uparrow}$ become smaller and smaller with $Z_{xz/yz\uparrow} < Z_{xy\uparrow}$ when U increases. This indicates that the SDW gap opening mainly occurs in the xz/yz orbitals.

The evolution of the PDOS with Coulomb interactions U is also displayed in figure 8. We find that at $U = 2.0$ eV and 3.0 eV there are obvious spin polarizations in the SAFM phase due to the breakdown of spin symmetry. The xz and yz orbitals dominate the FS, while the xy orbital mainly lies far from the Fermi level. This also shows that the xz/yz orbitals determine the electronic properties near E_F, and are mainly involved with the formation of the SDW states, consistent with the result of the renormalization factor in figure 7.

Since the electronic correlation is intermediate, one expects that U is larger than 2 eV in iron pnictides and selenides; thus at 2/3 filling, the SAFM state with orbital ordering is stable over a wide electron correlation range, from intermediate to strong correlations, which is similar to the FeAs-based systems.

3.3. Half-filling case

When turning to the half-filling case, which corresponds to the Fe^{3+}-based systems, such as $KFeSe_2$ and FeAs compounds, etc, we find that the phase diagram becomes much richer. It is found that there exist three critical points when U increases: the system transits from a PM metal to an SAFM metal at U_{c_1}, from an SAFM metal to a Néel AFM metallic phase at U_{c_2}, and from an AFM metal with intermediate-spin state to an AFM-OSMP with high-spin state at U_{c_3}, as shown in figure 9. These phases will be addressed in detail in the following. In comparison with the $n = 4.5$ and 4 cases, we find that besides the PM and SAFM phases, the Néel AFM metallic phase appears in a slightly large U region at $U_{c_2} \approx 0.8$ eV. Only when in the narrow Coulomb interaction region at $U_{c_1} \approx 0.65 < U < U_{c_2}$ is the SAFM phase stable, as the dependence of the boson occupancies on Coulomb interaction U show in figure 9. The ground-state energies of the SAFM and Néel AFM states with respect to the PM state as a function of U are plotted in the inset of figure 9. We can clearly see that the spin state transition at U_{c_2} is accompanied by a variation of the orbital polarization/order, indicating that the spin state transition is a first-order one, as seen in figure 10. With the increase of the Coulomb interaction, the triple occupation $r_{\downarrow\downarrow\downarrow}$ sharply increases, while the other high occupations are relatively small. This shows that the system undergoes a spin state transition with an increasing Coulomb interaction and Hund's rule coupling, as we see in the low-spin ($S = 1/2$) to intermediate-spin ($S = 1$) transition at U_{c_2} in figure 10.

On the other hand, the dependence of the orbital occupations and the magnetic moments of the three orbitals on the Coulomb interaction U is plotted in the left panel of figure 10. We find that in the SAFM phase a small orbital polarization appears with $n_{yz} > n_{xz}$ in the present hole representation, i.e. $n_{xz} > n_{yz}$ in the electron representation. This supports the itinerant orbital ordering in the parent phases of iron pnictides [26, 39]. Also, the magnetic moments on different orbitals possess $m_{yz} < m_{xz}$ with total magnetic moment $m_{tot} < 1\ \mu_B$. The system lies in a low-spin state. However, in the Néel AFM metallic phase, there is no orbital polarization, since in the presence of the spin–orbital coupling, the preserved spin rotational symmetry does not lift the orbital degeneracy or break the orbital symmetry. When $U > U_{c_3}$, the system enters the OSMP, as shown in the left panel of figure 10. All of the three-orbital occupations are

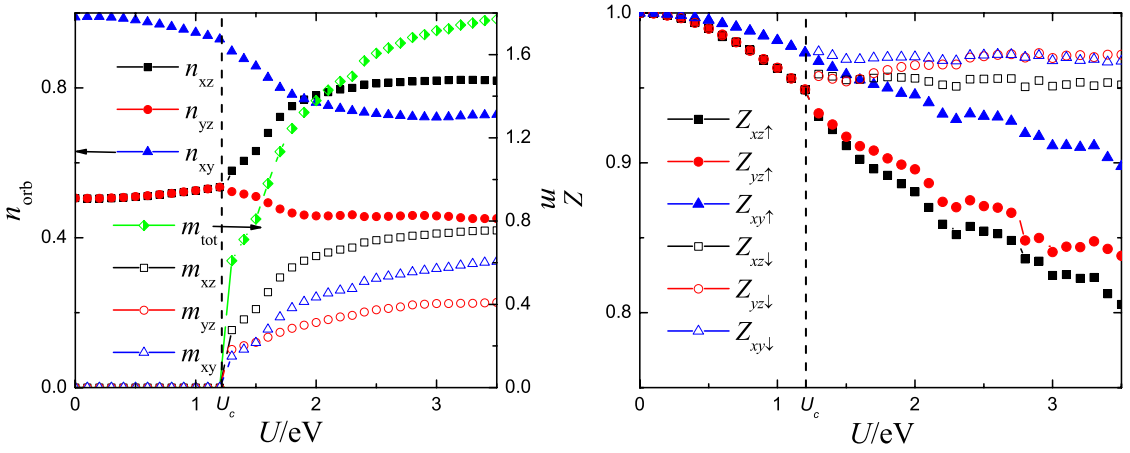

Figure 7. Dependence of orbital occupations and magnetic moment of each orbital (left panel) and renormalization factor (right panel) on the Coulomb interaction U at $n = 4$, and $J_H = 0.25U$.

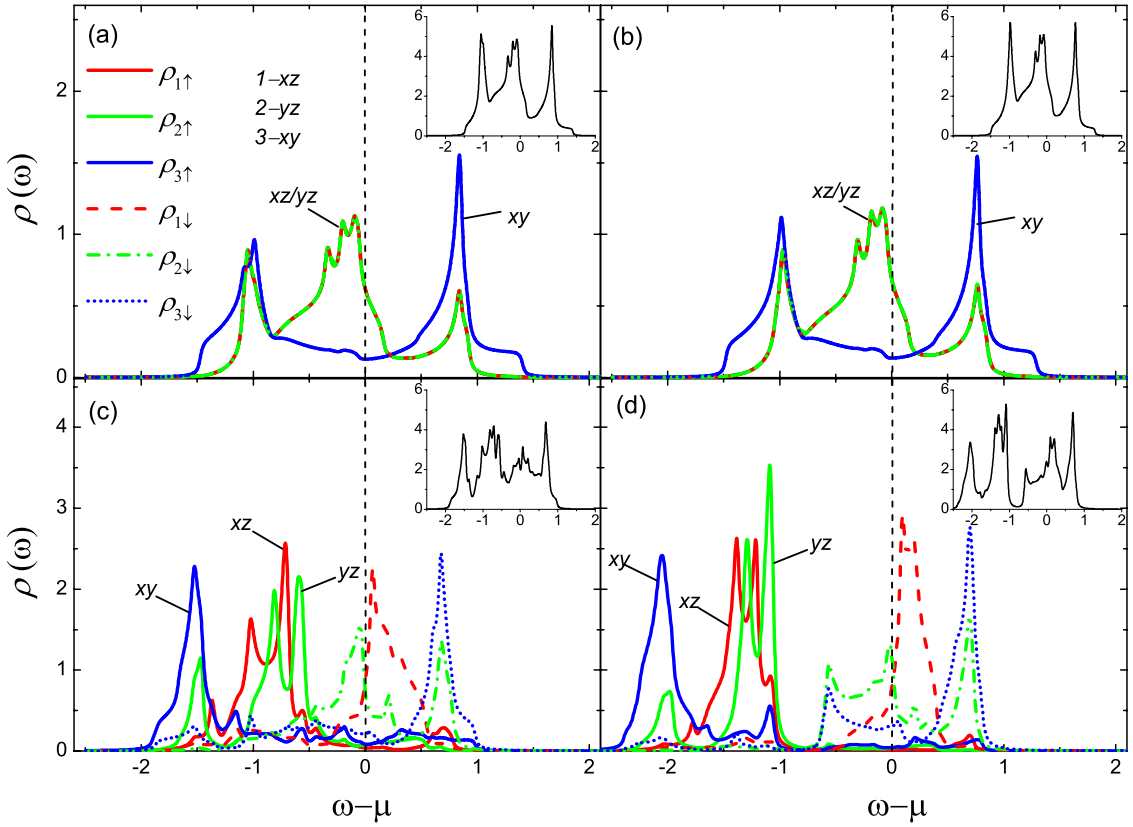

Figure 8. Projected densities of states are plotted for $U = 0$ (a), 1.0 eV (b), 2.0 eV (c), and 3.0 eV (d) at $n = 4$, respectively, with $J_H = 0.25U$. Inset: total densities of states.

nearly equal to 1. The magnetic moment per orbital steeply increases and the total magnetic moment m_{tot} is larger than 2 μ_B. Meanwhile, the system undergoes an intermediate-spin ($S = 1$) to high-spin ($S = 3/2$) transition with increasing U, and thus enters a high-spin state when $U > U_{c_3}$.

The right panel of figure 10 shows the renormalization factor of each orbital as a function of Coulomb interaction U, which is in sharp contrast with the $n = 4.5$ and 4 cases. In the PM and SAFM phases, all the renormalization factors Z_{xz}, Z_{yz} and Z_{xy} ($Z_{xz/yz} < Z_{xy}$) smoothly decrease with increasing U, indicating the bandwidths become narrow due to the increase of the Coulomb correlation. When $U > U_{c_2}$, the system enters the Néel AFM state. In this situation Z_{xy} gradually decreases, while Z_{xz} and Z_{yz} considerably change with U, suggesting that the variations of orbital and magnetic states mainly occur in these two orbitals. The lift of Z_{xz} and Z_{yz} implies the bandwidths of the two orbitals anomalously increase, which is attributed to the fact that the exchange splitting of spin-up and spin-down subbands of the xz and yz orbitals increases with

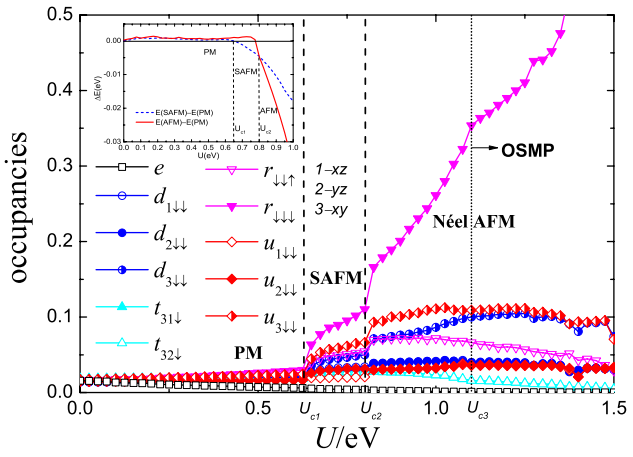

Figure 9. Dependence of boson occupancies on the Coulomb interaction U at half-filling $n = 3$ and $J_H = 0.25U$. Three dashed vertical lines denote the phase boundaries of the PM-SAFM, SAFM-Néel AFM, and Néel AFM-OSMP transitions at U_{c_1}, U_{c_2} and U_{c_3}, respectively. Inset: ground-state energies of the SAFM (dashed line) and Néel AFM (solid line) states with respect to the PM state as a function of U.

the increase of U, leading to the total bandwidth broadening, which is also seen in figure 11.

We present the PDOS of four typical phases, including PM, SAFM, Néel AFM metal and AFM-OSMP, in figure 11 for Coulomb interaction $U = 0$, 0.75, 1.0 and 1.5 eV, respectively. It is found that in a relatively small U region, i.e. $U \leq U_{c_2}$, the xz/yz orbitals dominate the FS in both the PM and SAFM phases. Different from figure 11(a), in the SAFM phase with $U = 0.75$ eV in figure 11(b), the orbital degeneracy between xz and yz orbitals is lifted, consistent with the orbital polarization in the left panel of figure 10. Meanwhile in the Néel AFM metallic state with $U = 1.0$ eV in figure 11(c), the weight of the xz and yz orbitals in the FS is greatly suppressed, but the spin splitting becomes large, consistent with the intermediate-spin configuration in figure 10. Interestingly, we find that when $U > U_{c_3} \approx 1.1$ eV, an orbital selective Mott transition (OSMT) occurs, i.e. an OSMP emerges. In this situation, only the broad xy orbital contributes to the FS, while the narrow xz and yz orbitals are insulating and sink below the FS, as seen in the PDOS with $U = 1.5$ eV in figure 11(d).

Therefore, at a half-filling, the system is mainly a Néel AFM state without orbital ordering in the intermediate and strong correlations, in addition to an OSMP phase related to an intermediate-spin to high-spin transition. Compared with the other band fillings, the different magnetic phase diagrams suggest a band filling controlling magnetism scenario in the iron selenide systems.

4. Discussion and summary

The scenario of OSMT in $K_xFe_{2-y}Se_2$ could be understood using a sketch of OSMP in the presence of magnetism, as shown in figure 12. When tuning to the half-filling, with the increase of Coulomb interaction and Hund's rule coupling, the spin-up and spin-down subbands split from each other; the spin-up xz- and yz-orbitals are filled, sink below E_F and become insulating; and the xy-orbital remains across E_F and is conducting, giving rise to an AFM-OSMP. We notice that in comparison with the bandwidths of $K_xFe_{2-y}Se_2$, the U_{c_3} for the occurrence of the OSMP is small. This may arise from the following two reasons: (1) in the parent phase of Fe-based superconductors, the Hund's rule coupling is large with $J_H = 0.25U$. If small values $J_H = 0.15U$ or $0.1U$ are adopted, U_{c_3} will reach relatively large values up to 2 or even 3 eV; (2) U_{c_3} is obtained for the OSMP with AFM order in the present study, it will become larger in the PM situation. Since $KFeSe_2$ possesses not only a tetrahedral crystal field but also a large magnetic moment, it may be a potential candidate for such an OSMP. Moreover, an OSMP was also observed in iron selenides under high pressure in a recent experiment [40]. We expect that further increasing the Coulomb interaction U will

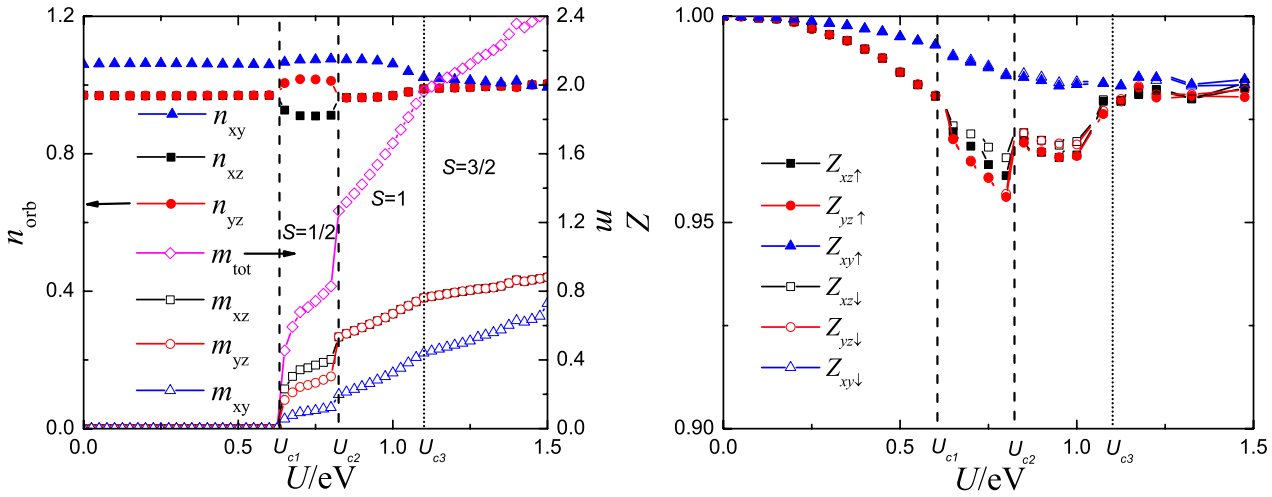

Figure 10. Orbital occupations and magnetic moment of each orbital (left panel), and renormalization factor (right panel) as a function of Coulomb interaction U at half-filling $n = 3$, and $J_H = 0.25U$. The dashed lines indicate the phase boundaries U_{c_1}, U_{c_2} and U_{c_3}.

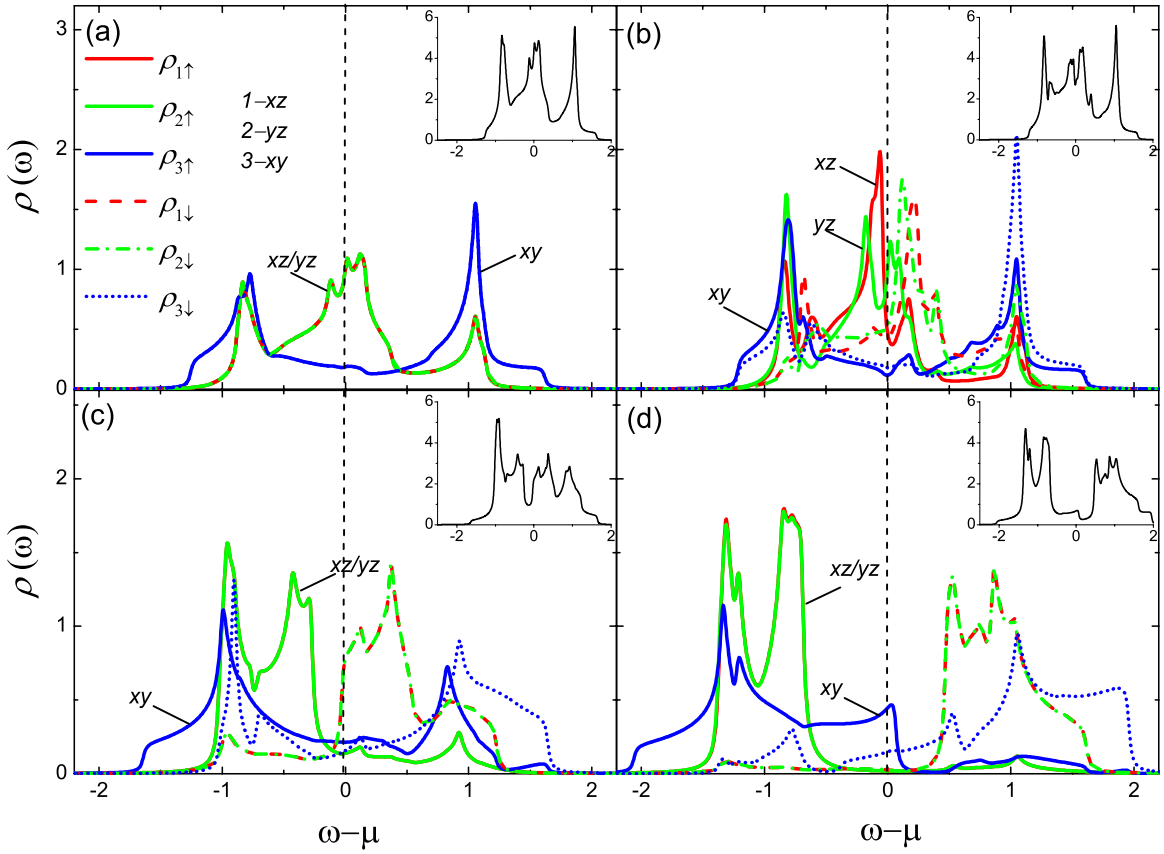

Figure 11. Projected densities of states are plotted for $U = 0$ (a), 0.75 eV (b), 1.0 eV (c), and 1.5 eV (d) at half-filling $n = 3$, respectively. $J_H = 0.25U$. Inset: total densities of states.

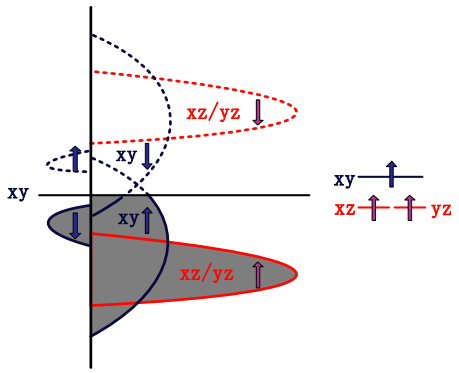

Figure 12. Sketch of sublattice band structures in the orbital selective Mott phase with Néel antiferromagnetism for the half-filled three-orbital model in $K_xFe_{2-y}Se_2$.

drive the system to a magnetic insulating state accompanied with a metal–insulator transition.

We notice that different from our PM results, the first-principles electronic structure calculations suggested the ground state in KFe_2Se_2 is the SAFM ordering [9], or the bi-collinear AFM ordering resulting from the interplay among the nearest, the next-nearest, and the next-next-nearest-neighbor superexchange interactions mediated by Se 4p-orbitals in AFe_2Se_2 (A = K, Tl, Rb, or Cs) [8]. In addition, some other iron-based materials, such as FeSe [41, 42], LiFeAs [43], and KFe_2As_2 [43–45], have no magnetism at all as observed in the experiments, but AFM is obtained in the LDA calculations. The discrepancies among these materials suggest the magnetism is sensitive to the electronic properties or lattice distortion [43]. Note that we do not consider the possibility of a spiral spin ground state in the present study. In a spin frustrated metal, the spiral spin state is stable in the weak and intermediate correlated regime, as Arrigoni *et al* [46] and Capone *et al* [47] pointed out. The stability of such a spiral state in $K_xFe_{2-y}Se_2$ deserves to be considered in a future study. The LDA methods usually overestimate the magnetic moment and AFM ordering but omit some spin fluctuations of the system due to the intermediate electronic correlation so that a proper treatment on the electronic correlation in these FeSe-based compounds may be important to understand its magnetic ground state. In our study, we deal with the electronic correlation within the framework of the KRSB approach, which is verified as an effective approach to treat electronic correlations ranging from weak through intermediate to strong ones. Our PM ground-state result, not a nonmagnetic one, indicates that there exists a strong spin fluctuation, which is regarded as the superconducting pairing mechanism, thus KFe_2Se_2 is a potential candidate for the parent phase for a superconductor without doping. Moreover, a recent STS experiment demonstrated the existence of phase separation and distinguished the contributions: the KFe_2Se_2 component contributes to superconductivity, while

the $K_{0.8}Fe_{1.6}Se_2$ Fe-vacancy ordering component contributes to the insulating properties [14], suggesting that pure KFe_2Se_2 is more possibly a PM phase when in the normal state. These observations are consistent with our present results.

In summary, starting with an effective three-orbital model for the newly found KFe_2Se_2, we have shown that the ground state of KFe_2Se_2 at three quarter filling is a paramagnetic metallic phase. We also suggest a possible OSMP phase through tuning the band filling in $K_xFe_{2-y}Se_2$. Our results demonstrate that the band filling plays a key role in the electronic and magnetic properties of $K_xFe_{2-y}Se_2$. Since the chemical phase separation widely exists in $K_xFe_{2-y}Se_2$ materials, future experiments are expected to confirm the magnetic ground state of KFe_2Se_2. In addition, the influence of the band filling and correlation on the electronic structures and magnetic properties in the presence of Fe vacancies for $K_xFe_{2-y}Se_2$ is an interesting topic, thus further theoretical works are expected.

Acknowledgments

The author (DY) gratefully acknowledges the help of Da-Mei Zhu with the manuscript. This work was supported by the Natural Science Foundation of China (NSFC) Nos 11104274, 11074257, 11204311, 11274310 and of Anhui Province No. 11040606Q56, and the Knowledge Innovation Program of the Chinese Academy of Sciences. Numerical calculations were performed at the Center for Computational Science of CASHIPS.

References

[1] Guo J G, Jin S F, Wang G, Wang S C, Zhu K X, Zhou T T, He M and Chen X L 2010 *Phys. Rev.* B **82** 180520
[2] Fang M H, Wang H D, Dong C H, Li Z J, Feng C M, Chen J and Yuan H Q 2011 *Europhys. Lett.* **94** 27009
[3] Wang Z, Song Y J, Shi H L, Wang Z W, Chen Z, Tian H F, Chen G F, Guo J G, Yang H X and Li J Q 2011 *Phys. Rev.* B **83** 140505
[4] Bao W, Huang Q Z, Chen G F, Green M A, Wang D M, He J B, Wang X Q and Qiu Y 2011 *Chin. Phys. Lett.* **28** 086104
[5] Ye F, Chi S, Bao W, Wang X F, Ying J J, Chen X H, Wang H D, Dong C H and Fang M H 2011 *Phys. Rev. Lett.* **107** 137003
[6] Zhang Y *et al* 2011 *Nature Mater.* **10** 273
[7] Qian T *et al* 2011 *Phys. Rev. Lett.* **106** 187001
[8] Yan X W, Gao M, Lu Z Y and Xiang T 2011 *Phys. Rev.* B **84** 054502
[9] Cao C and Dai J H 2011 *Chin. Phys. Lett.* **28** 057402
[10] Bao W *et al* 2009 *Phys. Rev. Lett.* **102** 247001
[11] Zhang L J and Singh D J 2009 *Phys. Rev.* B **79** 094528
[12] Liu D Y, Quan Y M, Zeng Z and Zou L J 2012 *Physica* B **407** 1139
[13] Maier T A, Graser S, Hirschfeld P J and Scalapino D J 2011 *Phys. Rev.* B **83** 100515
[14] Li W *et al* 2011 *Nature Phys.* **8** 126
[15] Yan Y J, Zhang M, Wang A F, Ying J J, Li Z Y, Qin W, Luo X G, Li J Q, Hu J P and Chen X H 2012 *Sci. Rep.* **2** 212
[16] Chen F *et al* 2011 *Phys. Rev.* X **1** 021020
[17] Li C H, Shen B, Han F, Zhu X Y and Wen H H 2011 *Phys. Rev.* B **83** 184521
[18] Cai P, Ye C, Ruan W, Zhou X D, Wang A F, Zhang M, Chen X H and Wang Y Y 2012 *Phys. Rev.* B **85** 094512
[19] Yuan R H, Dong T, Song Y J, Zheng P, Chen G F, Hu J P, Li J Q and Wang N L 2012 *Sci. Rep.* **2** 221
[20] Zhang A M, Xia T L, Tong W, Yang Z R and Zhang Q M 2013 *Sci. Rep.* **3** 1216
[21] Zhao J, Cao H B, Bourret-Courchesne E, Lee D H and Birgeneau R J 2012 *Phys. Rev. Lett.* **109** 267003
[22] Quan Y M, Zou L J, Liu D Y and Lin H Q 2012 *J. Phys.: Condens. Matter* **24** 085603
[23] Bünemann J, Weber W and Gebhard F 1998 *Phys. Rev.* B **57** 6896
[24] Bünemann J and Gebhard F 2007 *Phys. Rev.* B **76** 193104
[25] Kotliar G and Ruckenstein A E 1986 *Phys. Rev. Lett.* **57** 1362
[26] Quan Y M, Zou L J, Liu D Y and Lin H Q 2012 *Eur. Phys. J.* B **85** 55
[27] Fang C, Wu Y L, Thomale R, Bernevig B A and Hu J P 2011 *Phys. Rev.* X **1** 011009
[28] Lee P A and Wen X G 2008 *Phys. Rev.* B **78** 144517
[29] Krüger F, Kumar S, Zaanen J and van den Brink J 2009 *Phys. Rev.* B **79** 054504
[30] Yu S L, Kang J and Li J X 2009 *Phys. Rev.* B **79** 064517
[31] Daghofer M, Nicholson A, Moreo A and Dagotto E 2010 *Phys. Rev.* B **81** 014511
[32] Zhou S and Wang Z Q 2010 *Phys. Rev. Lett.* **105** 096401
[33] Graser S, Kemper A F, Maier T A, Cheng H P, Hirschfeld P J and Scalapino D J 2010 *Phys. Rev.* B **81** 214503
[34] Foo M L, Wang Y Y, Watauchi S, Zandbergen H W, He T, Cava R J and Ong N P 2004 *Phys. Rev. Lett.* **92** 247001
[35] Huang S M and Mou C Y 2011 *Phys. Rev.* B **84** 184521
[36] Brouet V, Marsi M, Mansart B, Nicolaou A, Taleb-Ibrahimi A, Le Févre P, Bertran F, Rullier-Albenque F, Forget A and Colson D 2009 *Phys. Rev.* B **80** 165115
[37] Shishido H *et al* 2010 *Phys. Rev. Lett.* **104** 057008
[38] Raghu S, Qi X L, Liu C X, Scalapino D J and Zhang S C 2008 *Phys. Rev.* B **77** 220503
[39] Liu D Y, Quan Y M, Chen D M, Zou L J and Lin H Q 2011 *Phys. Rev.* B **84** 064435
[40] Gao P W *et al* 2012 arXiv:1209.1340
[41] Ma F J, Ji W, Hu J P, Lu Z Y and Xiang T 2009 *Phys. Rev. Lett.* **102** 177003
[42] Imai T, Ahilan K, Ning F L, McQueen T M and Cava R J 2009 *Phys. Rev. Lett.* **102** 177005
[43] Yin Z P, Haule K and Kotliar G 2011 *Nature Mater.* **10** 932
[44] Sato T *et al* 2009 *Phys. Rev. Lett.* **103** 047002
[45] Lee C H *et al* 2011 *Phys. Rev. Lett.* **106** 067003
[46] Arrigoni E and Strinati G C 1991 *Phys. Rev.* B **44** 7455
[47] Capone M, Capriotti L, Becca F and Caprara S 2001 *Phys. Rev.* B **63** 085104